Evaluation of Physical and Chemical Properties of Residue from Gasification of Biomass Wastes

Sieradzka, Malgorzata; Mlonka-Medrala, Agata; Kalemba-Rec, Izabela; Reinmöller, Markus; Kuster, Felix; Kalawa, Wojciech; Magdziarz, Aneta

Published in:
Energies

Link to article, DOI:
10.3390/en15103539

Publication date:
2022

Document Version
Publisher's PDF, also known as Version of record

energies

MDPI

Article

Evaluation of Physical and Chemical Properties of Residue from Gasification of Biomass Wastes

Małgorzata Sieradzka [1,*], Agata Mlonka-Mędrala [2], Izabela Kalemba-Rec [1], Markus Reinmöller [3], Felix Küster [4], Wojciech Kalawa [2] and Aneta Magdziarz [1]

1 AGH University of Science and Technology, Faculty of Metals Engineering and Industrial Computer Science, Mickiewicza 30 Av., 30-059 Krakow, Poland; kalemba@agh.edu.pl (I.K.-R.); amagdzia@agh.edu.pl (A.M.)
2 AGH University of Science and Technology, Faculty of Energy and Fuels, Mickiewicza 30 Av., 30-059 Krakow, Poland; amlonka@agh.edu.pl (A.M.-M.); kalawa@agh.edu.pl (W.K.)
3 DTU Engineering Technology, Technical University of Denmark, Lautrupvang 15, 2750 Ballerup, Denmark; markre@dtu.dk
4 Institute of Energy Process Engineering and Chemical Engineering (IEC), TU Bergakademie Freiberg, Fuchsmuehlenweg 9, 09599 Freiberg, Germany; felix.kuester@iec.tu-freiberg.de
* Correspondence: msieradz@agh.edu.pl

Abstract: Thermochemical conversion of biomass waste is a high potential option for increasing usage of renewable energy sources and transferring wastes into the circular economy. This work focuses on the evaluation of the energetic and adsorption properties of solid residue (char) of the gasification process. Gasification experiments of biomass wastes (wheat straw, hay and pine sawdust) were carried out in a vertical fixed bed reactor, under a CO_2 atmosphere and at various temperatures (800, 900 and 1000 °C). The analysis of the energy properties of the obtained chars included elemental and thermogravimetric (TGA) analysis. TGA results indicated that the chars have properties similar to those of coal; subjected data were used to calculate key combustion parameters. As part of the analysis of adsorption properties, BET, SEM, FTIR and dynamic methanol vapor sorption tests were conducted. The specific surface area has risen from 0.42–1.91 m^2/g (biomass) to 419–891 m^2/g (char). FTIR spectroscopy confirmed the influence of gasification on the decomposition of characteristic chemical compounds for biomass. Methanol sorption has revealed for the 900 °C chars of pine sawdust the highest sorption capacity and its mass change was 24.15% at P/P_0 = 90%. Selected chars might be an appropriate material for volatile organic compounds sorption.

Keywords: CO_2-gasification; biomass wastes; char adsorption; active carbon; BET specific surface area

Citation: Sieradzka, M.; Mlonka-Mędrala, A.; Kalemba-Rec, I.; Reinmöller, M.; Küster, F.; Kalawa, W.; Magdziarz, A. Evaluation of Physical and Chemical Properties of Residue from Gasification of Biomass Wastes. *Energies* **2022**, *15*, 3539. https://doi.org/10.3390/en15103539

Academic Editor: Alok Kumar Patel

Received: 12 April 2022
Accepted: 9 May 2022
Published: 12 May 2022

1. Introduction

Modern challenges are related to the limited amount of fossil fuels, greenhouse gas emissions directly related to the consumption of fossil fuels in various forms [1], as well as the improvement of waste management policies towards the circular economy [2]. For this reason, it is necessary to take quick, decisive and wise steps to use renewable energy (RE) sources, such as biomass, to generate clean energy, as well as improve waste management by using different types of waste, such as RE, and minimizing the waste resulting from their production. Biomass as a renewable energy source has enormous potential. It can be converted by thermochemical processes such as pyrolysis [3,4], hydrothermal carbonization [5,6] or gasification [7], which allows the production of clean energy resources. This study is focused on the gasification process, where the main product is the synthesis gas (syngas) [8,9]. The applied process temperature depends on the material to be gasified and the targeted gas composition. Gasification can be carried out in a temperature range of 600 to 1600 °C in the case of municipal solid waste (MSW) [10,11], in the case of biomass the process temperature range is lower and its ranges vary from 400 to 1100 °C [12,13]. Some of the most commonly used gasifying agents are steam, carbon dioxide and air [14]. This

process leads to the formation of gaseous (syngas), liquid (tar) and solid (char) products at lower/moderate gasification temperatures. However, any remaining solids from this process are normally treated as waste [15], leading to a decrease in process efficiency and an increase in waste production. Current studies indicate that gasification chars have a huge potential, both energetic and adsorptive, as a precursor to the formation of activated carbon (AC) [15,16].

AC is characterized by a high surface area, which indicates its great adsorption capacity. Generally, the production and regeneration costs of AC are high, and because of that it is important to find a cheaper way to produce this key solid carrier [17]. The key properties of AC are the small ash content, the ability to maintain physiological characteristics, hardness, and a high carbon content [18]. Figure 1 presents the main steps of AC synthesis; they include preliminary, carbonization, and activation steps. Within the preliminary step, removal of impurities from raw material is provided by washing, then it is dried to remove moisture [19], to obtain similar particle sizes, the raw material is milled and sieved [20], and in the last stage of this step it might be deashed for demineralization by acidic or basic solutions [21]. Volatile matter is removed from raw material during the carbonization step, leading to an increase in carbon concentration in the material produced [22]. After the second stage, a porous structure is formed; it can be developed through physical and chemical activation [17].

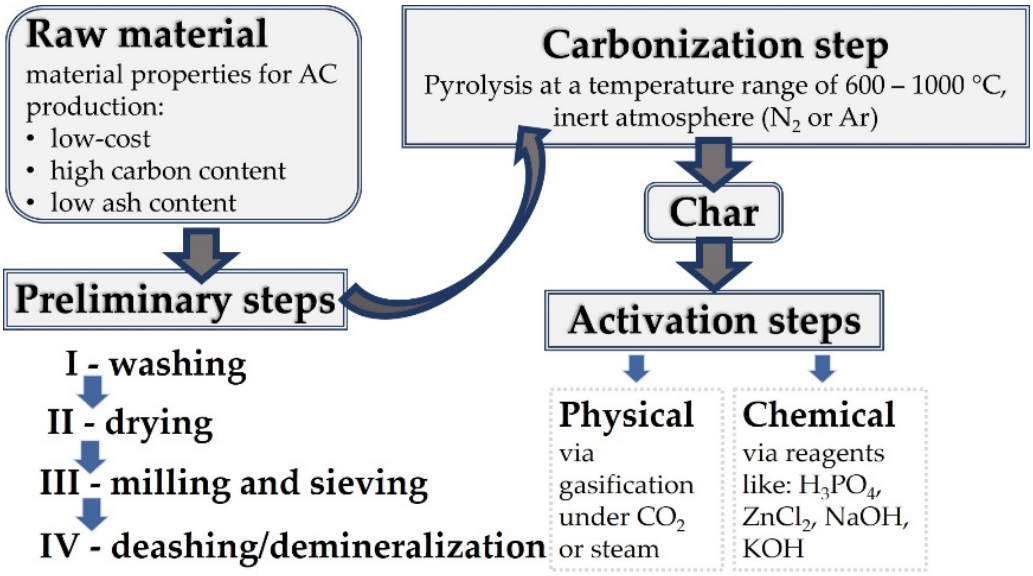

Figure 1. Pathway of activated carbon formation.

The production of activated carbon via physical activation depends on the type of material, the high temperature, the atmosphere with oxidizing gases such as steam, CO_2 or air, and leads to the production of expanded pores structure through the carbon-consuming Reactions (1)–(3) [17]:

$$C + O_2 \rightarrow CO_2 \quad (1)$$

$$C + CO_2 \rightarrow 2CO \quad (2)$$

$$C + H_2O \rightarrow CO_2 + 2H_2 \quad (3)$$

Activated carbon produced by chemical activation includes biomass impregnation via a dehydrating chemical agent, like phosphoric acid, sulphuric acid or zinc chloride in an inert atmosphere by heat treatment. This leads to the production of activated carbon with a large pore structure, which is a desired phenomenon [20].

In a number of studies, the similarities between gasification chars and activated carbon are indicated: Benedetti et al. [15] have pointed out an analogy of gasification char properties to activated carbon (AC) and reviewed its successful applications in the field

of adsorption. They used a few chars obtained from gasification plants in the process of conversion of wood chips and pellets after gasification under air at various temperatures (650–900 °C). The main conclusion of this study was that chars are very similar to AC, however, a detailed analysis of each sample is necessary to choose the most suitable application. Benedetti et al. [23] have focused on the gasification char CO_2 adsorption/desorption capacity. The final results indicated that chars obtained from gasification plants offer significant potential in carbon capture storage (CCS) technology. The ability of gasification chars to remove cationic, crystal violet, and anionic congo red chars obtained from industrial gasification of municipal solid waste (MSW) was investigated by Jung et al. [24]. This study indicates that these types of chars have high potential for applications of adsorption in wastewater treatment. AC obtained from gasification chars has the ability to remove H_2S (hydrogen sulphide). This is a common pollutant in biogas produced during anaerobic digestion and syngas obtained from gasification. This capability of gasification chars was studied in other work [25].

The gasification process is an effective waste conversion method. It leads to the production of valuable syngas and solid residues. Syngas analysis has been widely investigated in other works [14,26]. In the presented study, the main focus was on the analysis of solid residue, which is considered as a waste. The two main aims of this study were proposed. First, the energetic properties of the chars obtained from the gasification process were investigated. Second, as other studies conducted, each char mimics activated carbon properties, and individual analysis is required to choose the most adequate application in the adsorption area. Therefore, in this study, the chars formed during the gasification process of waste biomass were examined in terms of methanol adsorption. Methanol is one of the typical volatile organic compounds (VOCs), leading to serious health issues [27]. Another possible utilization of the produced solid residue is in a working pair with methanol in heat-driven sorption cooling devices.

2. Materials and Methods

2.1. Materials

In this study, two types of biomass wastes were selected (agriculture: wheat straw (ABW) and hay (ABH); wood: pine sawdust (WBP)). The materials used in the experiments were dried first and after that independently ground by a knife mill to achieve a similar particle size.

2.2. Test Rig and Experimental Procedure

Gasification experiments were conducted under CO_2 atmosphere at three temperatures of 800, 900, and 1000 °C. During the process, formed syngas was collected and analysed. This paper is focused on solid residue and its properties, and because of that, syngas analysis was omitted. The test rig overview scheme is presented in Figure 2. The gasifier consists of a fixed-bed vertical quartz reactor heated by a furnace to the target temperature. The maximum furnace power was 1.8 kW and was equipped with a (NiCr-NiAl) type thermocouple, which allowed the process temperature to be controlled in real time. The process atmosphere was injected from an external cylinder with a high purity of CO_2, while the flow of the gasification agent was controlled by a rotameter.

The experimental procedure included the following steps: weighing the sample, weighing the quartz wool, placing the quartz wool and the sample in the reactor, assembling the reactor in the oven, providing the gasification process, cooling the oven, disassembling the reactor and weighing obtained chars. The input weight of the sample was constantly 8 g. Quartz wool was placed at the bottom of the sample to prevent the sample from falling to the bottom of the reactor and to ensure that it was located in the centre of the oven heating zone. Prior the gasification process, the reactor was flushed with pure CO_2 at ambient temperature, with a flow rate of 80 mL/min, for 15 min, to remove all air. Next, the sample was heated for 15 min, and once the set temperature was achieved the gasification process

was carried out for the next 15 min. Once the gasification process was finished, the reactor with the formed char was cooled to ambient temperature in a CO_2 atmosphere.

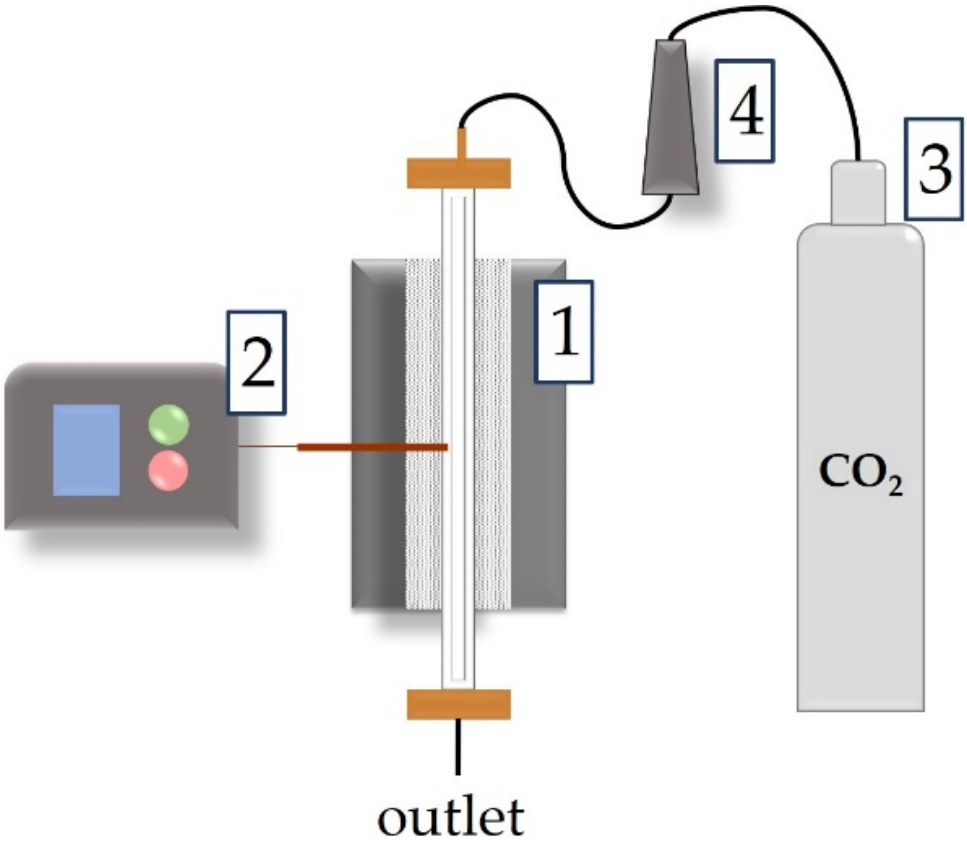

Figure 2. Scheme of the test rig: 1—fixed-bed vertical reactor, 2—temperature controller, 3—gas cylinder, 4—rotameter.

2.3. Analysis of Raw Materials and Chars

To determine raw material properties, proximate and elemental analyses of all samples were performed. Moisture (M), ash (A), and volatile matter (VM) content were established according to the following European standards: PN-EN ISO 18134-1:2015-11, PN-EN ISO 18122:2016-01, and PN-EN ISO 18123:2016-01, respectively. The elemental composition was investigated using a Truspec CHNS 628 Leco analyzer determining the contents of carbon (C), hydrogen (H) and nitrogen (N). The same analyzer was used to establish the elemental composition of the obtained chars. This apparatus has a standard deviation for carbon and nitrogen at a level of ±0.5% and for hydrogen at a level of ±1.0%. This device uses the Dumas method to establish the concentration of the elements mentioned above. It involves the combustion of the sample in pure oxygen at a temperature of 950 °C.

To indicate more valuable data on the energetic properties of materials, the higher heating value (HHV) in MJ/kg, was calculated based on the following equation [28]:

$$HHV = 5.22C^2 - 319C - 1647H + 38.6C{\cdot}H + 133N + 21028 \quad (4)$$

2.4. Thermogravimetric Analysis

A Mettler Toledo TGA/DSC 1 Star System thermogravimetric analyzer (TGA) was used to study the combustion process of the raw materials and the obtained chars. The analyses took place in air atmosphere and started from the ambient temperature up to 800 °C with a heating rate of 10 K/min. The mass sample was around 5 mg and placed in the platinum crucible.

2.5. Specific Surface Analysis (BET)

The Brunauer–Emmett–Teller (BET) method was used to determine specific surface areas in the raw biomass and the chars obtained. A nitrogen adsorption analyzer ASAP 2010 system (Micromeritics, Norcross, GA, USA) was used. Before analyses, all samples were pretreated with degasses to eliminate faults caused by other gases during the analysis. The studied samples were degassed for 24 h at a temperature of 200 °C in a case of raw biomass and at a temperature of 250 °C in a case of chars.

2.6. Fourier-Transformed Infrared Spectroscopy (FTIR)

The surface functional groups of the studied samples were found by Fourier-transformed infrared spectroscopy (FTIR). This apparatus analyzes the chemical groups of the biomass/char based on the characteristic vibrations of the chemical functional groups. The Bruker Alpha II system was applied in the range of collected spectra from 400 to 4000 cm^{-1}.

2.7. Scanning Electron Microscopy (SEM)

For the investigation of raw materials and chars obtained at a gasification temperature of 1000 °C, the morphology and surface topography were analyzed using a Nova NanoSEM 450 scanning electron microscopy (SEM). Analysis was carried out under high vacuum with a secondary electron detector with a voltage of 10 kV. In these analyses, chosen chars obtained at the highest process temperature are used to compare the modification of the raw material subjected to gasification.

2.8. Dynamic Methanol Vapor Sorption Tests

The Dynamic Gravimetric Vapor Sorption System DVS Vacuum was used for the investigation of the methanol adsorption properties of the studied samples. Methanol was selected as it is a nonhazardous and very common adsorbate used in sorption cooling devices in a working pair with activated carbon [27,29–31]. The mass of the sample was measured with high sensitivity (0.1 µg) by the apparatus during the adsorption and desorption processes. The stability of the temperature was equal to ±0.02 K, at 25 °C, where the humidity condition, with respect to the target value, was generated in the range of ±0.1% [32,33]. The DVS Vacuum allowed performing experiments of static and dynamic sorption with measurements of isotherms and isobars of adsorption–desorption over a wide range of temperatures.

In the presented study, methanol was used as an adsorbate. About 20 mg of produced char obtained at 900 °C was placed in a crucible and dried at 100 °C for approximately 60 min to achieve sample degassing. After a 60 min stabilization stage at given process temperature, a series of 18 experimental stages started. Each stage lasted 20 min and had a different setting of a relative pressure P/P_0, starting from 10% to 90%. Based on the obtained results, adsorption and desorption isotherms were calculated. The methanol flow rate was set constant and equal to 15 sccm (standard cubic centimeters per minute). The experiment was carried out at adsorption temperature of 30 °C, and assumed desorption temperature of 60 °C [33].

3. Results and Discussion

3.1. Char as a Material with Energy Potential

3.1.1. Characterization of Raw Biomass and Chars

The main results of the elemental and proximate analysis of raw biomasses are presented in Table 1. The carbon content of the studied biomasses obtained the lowest value for ABH (39.6%) and the highest value for wood biomass WBP (48.6%). Its concentration after the gasification process increased significantly. The greatest change was observed for the ABH sample, which reached 92.1% for the char obtained at temperature 1000 °C. For other char samples, an increase in the process temperature results in a decrease in the C content from 76.8% to 71.7% for ABW and from 60.7% to 53.1% for WBP. Nitrogen content did not exceed 2%. In the case of hydrogen, a decrease in its content was noted

when comparing raw material with chars; this is related to the release of hydrocarbons that form syngas during gasification. When analyzing the results for the chars, the highest decrease occurred at a temperature of 1000 °C and it was 0.9% for ABW_1000 and 0.8% for ABH_1000 and WBP_1000.

Table 1. Raw biomass characterization.

	Raw Biomass		
	ABW	**ABH**	**WBP**
	Proximate Analysis (%)		
VM	74.06	59.94	79.89
A	3.86	21.83	0.19
M	4.99	7.71	6.76
FC	17.08	10.52	13.16
	Elemental Analysis (%) *		
C	44.65	39.59	48.56
H	6.47	5.76	6.57
N	0.68	1.16	0.07
O **	39.35	23.95	37.86

* moisture and ash-free. ** calculated by difference.

The results of the elemental analysis were used to calculate the hydrogen (H/C ratio) and oxygen (O/C ratio) indexes in the studied samples (Figure 3). Biomass is characterized by a high content of oxygen compared to coal, which influences its heating value. It is related to the fact that the strength of carbon–hydrogen and carbon–oxygen bonds is lower than that of carbon-carbon bonds [34]. The ratio of H/C and O/C in raw biomass was averaged at 1.7 and 0.7, respectively, indicating that the raw material has a low aromaticity and a high aliphatic content [35]. The results for the hydrogen and oxygen indexes of the chars decreased significantly, which indicates that it is more similar to the coal, where the H/C of the coal is in the range of 0.4–1 and the O/C is up to 0.2 [35]. Based on the results presented in Figure 3, it can be observed that the H/C and O/C values for the chars did not exceed the value of 0.2.

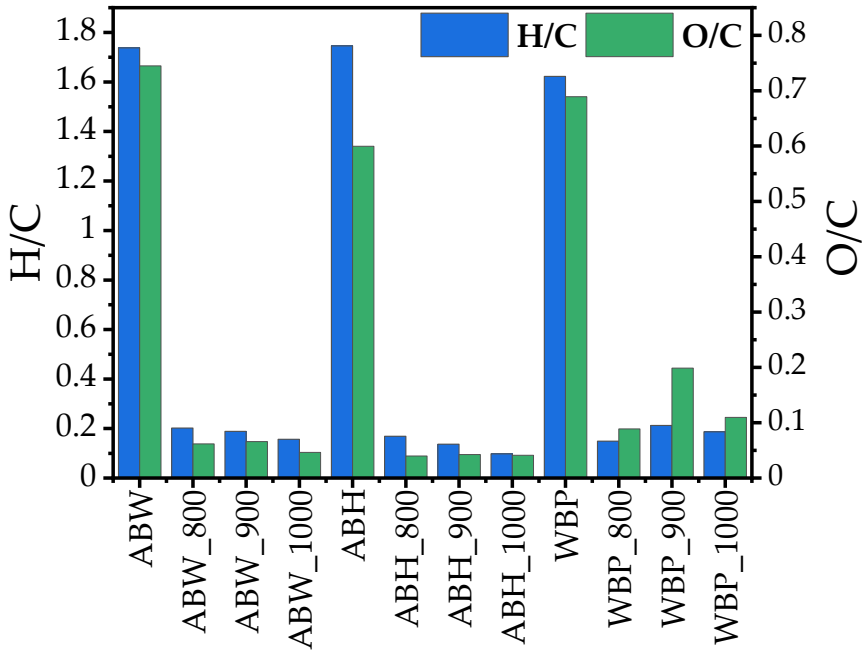

Figure 3. Hydrogen (H/C ratio) and oxygen (O/C ratio) indexes of the studied samples.

The influence of gasification temperature on char HHV and raw biomass HHV, as a reference, is presented in Table 2. Raw materials obtained HHV at a level of 17.8, 16 and 19.4 MJ/kg for ABW, ABH and WBP, respectively. For comparison, this value in other studies was 16.6 MJ/kg for mixed sawdust reported in [36], 19.9 MJ/kg for pine sawdust and 19.1 MJ/kg for chestnut sawdust reported in [37]. The HHV of millet husk char obtained from gasification was 22.9 MJ/kg [38]. In this study, a significant increase in HHV was observed for chars, especially for ABW and ABH samples. With an increase in the process temperature, there was a slight decrease in the HHV as a result of the higher release of carbon content towards syngas production. Additionally, the value of HHV for other carbonized materials and various types of carbon reported in [39] was 31.8 MJ/kg for anthracite coal, 18.5 MJ/kg for briquette, 35 MJ/kg for coal, 31.3 MJ/kg for lignite char and 34.4 MJ/kg for charcoal. When the results presented in other studies and the data obtained are analyzed, it can be concluded that chars have values similar to coal. The best results were obtained for the chars produced at a temperature of 800 °C.

Table 2. Higher heating value of studied samples.

Sample	HHV, MJ/kg
ABW	17.78
ABW_900	27.77
ABW_1000	26.25
ABH	16.05
ABH_800	38.12
ABH_900	37.46
ABH_1000	37.47
WBP	19.35
WBP_800	21.52
WBP_900	19.80
WBP_1000	19.33

Table 3 presents the yield of the char formation during gasification. An increase in process temperature leads to a decrease in the amount of solid residue. The highest values were obtained for the ABH sample, which contains the highest ash content (21.8%), where the WBP yield was the lowest, which corresponds to the lowest ash content (0.2%). In the case of ABH, the char yield decreased from 25.7% for 800 °C to 21.8% for 1000 °C. For WBP samples, for the same parameters, the char yields decreased from 15.3% to 13.1%. This phenomenon is related to an increase in char consumption during the Boudouard reaction due to the shift of the chemical equilibrium toward CO at higher temperatures [40].

Table 3. The yield of char formation during gasification.

Sample	Char Yield, %
ABW_800	21.0
ABW_900	17.4
ABW_1000	14.9
ABH_800	25.7
ABH_900	22.6
ABH_1000	21.8
WBP_800	15.3
WBP_900	13.2
WBP_1000	13.1

3.1.2. Thermogravimetric Analysis of Combustion Properties of Raw Biomasses and Chars

The comparison of the mass loss (TG curves) and the differential mass loss (DTG curves) of raw biomass and its chars during the combustion process is presented in Figure 4.

During the analysis, the combustion reaction occurred in different temperature zones for raw biomass samples than for chars obtained from it. There can be distinguished two stages of combustion in the case of raw biomass [41]: the first stage is related to the combustion of volatile matter and appeared in temperature zones of 160–330 °C for ABW, 135–330 °C for ABH and 160–360 °C for WBP, which can be observed based on DTG curves. The second stage appeared in temperature ranges 330–457 °C, 330–484 °C, 260–490 °C for ABW, ABH and WBP, respectively. The fact that the combustion process of the chars is missing the first stage is related to the fact that volatile matter was released during gasification. Its second stage appeared in approximate temperature ranges of 244–494 °C, 255–486 °C and 340–620 °C for ABW, ABH and WBP, correspondingly. When comparing the second stages of combustion of raw materials and chars, we can see a higher intensity at DTG peaks in this area for chars than for raw biomass. It is related to the fact that char contains a higher content of carbon, resulting in high-intensity combustion of carbon compounds at this stage. During combustion of raw material, volatiles start to evolve at a lower temperature and then burn in an area of higher temperature by reaching ignition temperature. Generated heat during volatile combustion influences the start of the combustion process of fixed carbon [42,43]. As the volatile matter was removed from the chars, it can be observed that only one peak is detected at the DTG curve, where the mass loss at the TG curve is moved to higher temperature areas.

On the basis of the TG and DTG results, the characteristic parameters like ignition temperature (T_i, °C), burnout temperature (T_b, °C), maximum mass loss rate ($(dW/dT)_{max}$, wt. %/min), average mass loss rate ($(dW/dT)_{av}$, wt. %/min) the temperature of the highest peak of DTG (T_{DTG}, °C), time corresponding to the parameters mentioned above, such as the ignition time (t_i, min), burnout time (t_b, min), time range = 0.5 ($\Delta t_{1/2}$, min) and the maximum peak time (t_p, min) were obtained and used in the calculation of key combustion parameters for all studied samples [44,45].

As described earlier, based on the characteristic parameters of the TG and DTG curves, the parameters were obtained based on the 'Intersection method' described in refs. [46,47]. The data was used to determine the key combustion parameters according to the following equations:

$$D_i = \frac{(dW/dT)_{max}}{t_p \cdot t_i} \quad (5)$$

$$D_f = \frac{(dW/dT)_{max}}{\Delta t_{1/2} \cdot t_p \cdot t_b} \quad (6)$$

$$S = \frac{(dW/dT)_{max} \cdot (dW/dT)_{av}}{T_i^2 \cdot T_b} \quad (7)$$

$$H_f = T_{DTG} \ln\left(\frac{\Delta t_{1/2}}{(dW/dT)_{av}}\right) \quad (8)$$

The group of key parameters includes the following indexes: ignition (D_i), burnout (D_f), comprehensive combustion characteristic (S), rate and intensity of combustion processes (H_f), which are described by the corresponding Equations (5)–(8) and its calculated values are presented in Table 4.

The ignition index D_i describes the ability to release volatile compounds from fuel, which also determines the stability of combustion [44,48]. With an increase in its value, this ability increases with increasing stability of combustion. Burnout performance, combustion intensity and reactivity are described by comprehensive combustion index S, where greater values characterise better combustion behaviour [48]. The rate and intensity of combustion is described by the H_f index, which additionally reflects the stability of the flame after ignition. A decrease in its value indicates a better combustion characteristic [49].

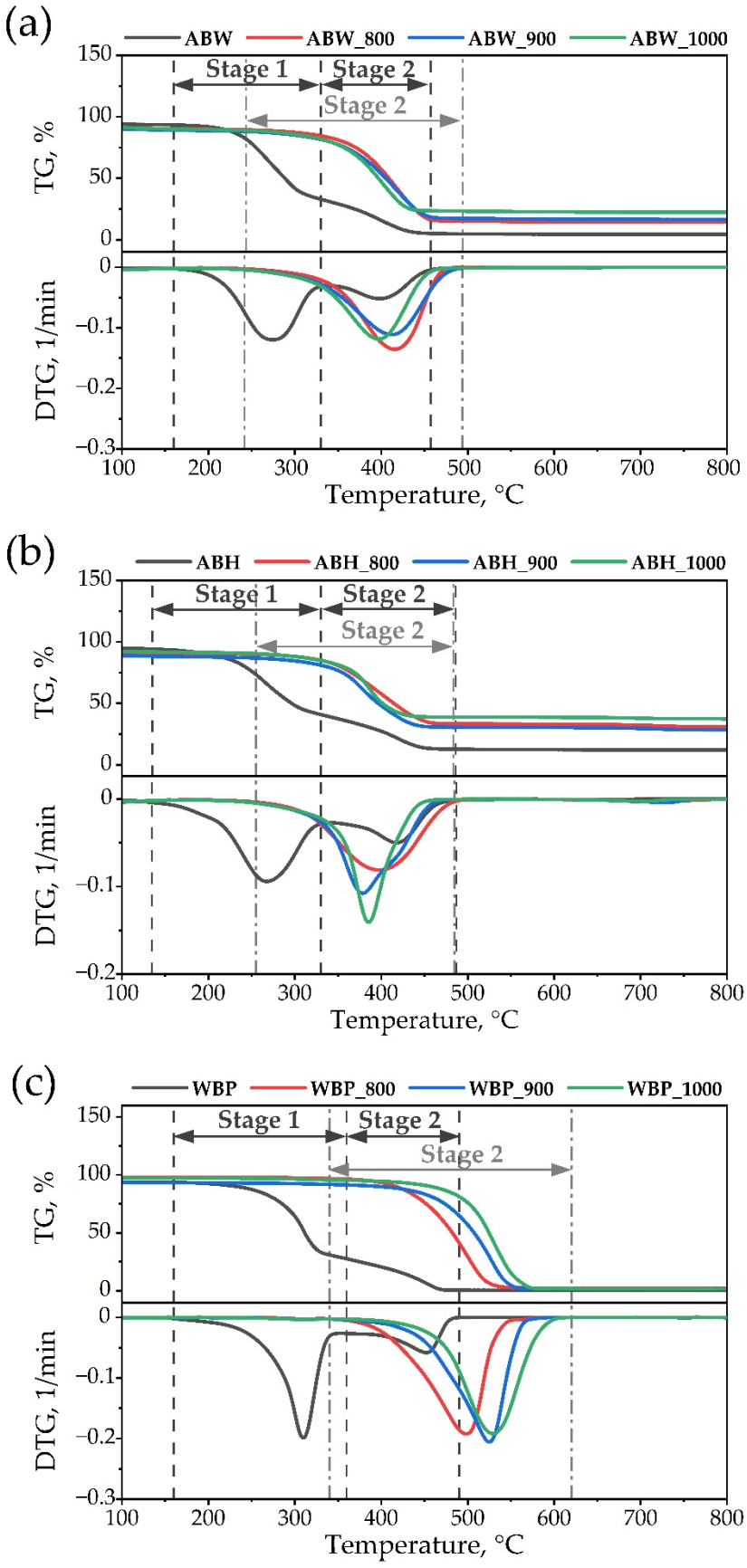

Figure 4. TG and DTG curves of (**a**) ABW, (**b**) ABH and (**c**) WBP.

Table 4. Key combustion parameters.

Sample	T_{ig}, °C	T_b, °C	D_i, wt. %/min^3	D_f, wt. %/min^4	S, min^{-2} °C^{-3}	H_f, °C
ABW	233.1	398.2	5.82×10^{-3}	1.55×10^{-4}	3.27×10^{-7}	966
ABH	222.6	417.7	4.84×10^{-3}	9.00×10^{-5}	2.48×10^{-7}	959
WBP	262.4	452.3	8.03×10^{-3}	1.33×10^{-4}	3.94×10^{-7}	1126
ABW_800	354.1	415.7	3.40×10^{-3}	6.29×10^{-5}	1.38×10^{-7}	1657
ABW_900	345.6	411.8	2.87×10^{-3}	5.37×10^{-5}	1.17×10^{-7}	1640
ABW_1000	339.8	397.1	3.20×10^{-3}	6.17×10^{-5}	1.24×10^{-7}	1606
ABH_800	335.7	397.7	2.23×10^{-3}	4.35×10^{-5}	0.79×10^{-7}	1644
ABH_900	338.6	378.5	3.03×10^{-3}	6.09×10^{-5}	1.10×10^{-7}	1559
ABH_1000	352.5	385.5	3.78×10^{-3}	7.48×10^{-5}	1.14×10^{-7}	1652
WBP_800	420.9	498.4	3.59×10^{-3}	5.57×10^{-5}	1.32×10^{-7}	2001
WBP_900	450.6	525.0	3.46×10^{-3}	5.13×10^{-5}	1.18×10^{-7}	2135
WBP_1000	486.9	529.1	3.01×10^{-3}	4.65×10^{-5}	0.93×10^{-7}	2161

The ignition process is reflected in the T_i parameter and the D_i index. This stage of combustion is boosted by the large amount of volatile matter in the sample, and results in a tendency to burn quickly [50]. As the VM are removed from the chars after gasification, it is expected that the ignition temperature increases for carbonized samples in comparison to the raw biomass. The range of T_i for raw biomass is 222–262 °C, while for chars it is 335–486 °C [51]. This trend indicates that char samples have lower reactivity, which is characteristic for coal [52]. The relationship between VM concentration and ignition performance is noticeable through results of D_i, where the value of this index is the highest for WBP (8.03×10^{-3}), which consists of almost 80% VM in raw form. Another factor affecting ignition temperature is the ash content, which decreases its values with increasing content. The concentration of ABH ash is 21.8%, where its T_i is the lowest of all the samples analysed (222.6 °C).

The burnout process is characterized by the D_f index, which is influenced not only by the temperature of T_b but also by the temperature of T_i. The lower the T_b temperature, the faster the burnout process is as the reduction of unburnt compounds is completed. A higher burnout temperature indicates that the process must be extended, which requires a higher temperature and a longer residence time [52]. This phenomenon is apparent when we analyse the T_b and D_f values for raw biomass and chars. In case of samples ABW and WBP, burnout temperature for its chars increased because of the difficulties in burning the carbonized samples, and the parallel burnout index value also increased. We observe an inverse relationship for the ABH sample, which contains the highest concentration of ash among all studied samples, which shortens the combustion process due to the lower content of combustible parts in the material. The better combustion process was determined by the S index; the increase in the value indicates rapid combustion with the release of a large amount of heat in a short range of time, which is characteristic for biomass. In the case of coal, this parameter is lower. The highest decrease in the S index is reported for the WBP sample where in raw form S is equal to 3.94×10^{-7} min^{-2} °C^{-3}, where in the case of WBP_1000 it is 0.93×10^{-7} min^{-2} °C^{-3}. Lastly, the H_f index shows an upward trend for chars. The range of the Hf index of raw biomass is 959–1126 °C, where for chars it is 1559–2161 °C. Mureddu et al. [52] have evaluated the combustion performance of different kinds of coals and biomasses. On the basis of these results, we can conclude that after the gasification process, the samples of chars are close to the combustible properties of coal.

3.2. Adsorption Properties of Chars

3.2.1. Surface Area (BET)

The surface area of the chars compared to the raw biomass samples measured by N_2 adsorption is shown in Table 5. Additionally, Table 5 indicates a literature review

of BET surface area (S_{BET}) of activated chars of different biomass samples via physical activation under different atmospheres and two commercial activated carbons. In the case of the studied raw biomass, S_{BET} has been reported as small values, where chars have exhibited a significant increase. The surface area varies from 469.6 to 891.5 m^2/g, from 256 to 419 m^2/g and from 520.9 to 764.8 m^2/g for chars obtained from ABW, ABH and WBP, respectively. These data indicate that ABH chars showed the lowest S_{BET} due to the highest mineral matter content (21.8%) [15]. The largest surface area was obtained for ABW chars. The increase of process temperature from 800 °C to 900 °C results in a higher surface area. This phenomenon is determined by the release of volatile matter contained in raw biomass. In the case of results for temperatures of 900 and 1000 °C, a decrease of S_{BET} for agriculture biomass was observed; for wood biomass the increase was not significant. Extensive heating of the samples provided for breaking and cracking of the pore structure [20] resulting in a reduction of the S_{BET} value from 891 to 624 m^2/g for ABW and from 419 to 296 m^2/g for ABH, in the case where the WBP value increases only 16 m^2/g. For comparison, the value of the surface area of the BET of biomass solid residue in the literature ranges from 167 to 1355 m^2/g, whereas the activated carbon BET ranges from 984 to 1002 m^2/g.

Table 5. BET analysis of raw biomass and chars.

Experiment		Literature Review			
Sample Name	**S_{BET} Surface Area, m^2/g**	**Raw Sample Name**	**Gasification Conditions**	**BET Surface Area, m^2/g**	**Ref.**
ABW	1.91	Chars			
ABH	1.25	Corn straw	99.9% CO_2, 800 °C	444	[53]
WBP	0.42	Poplar	90% CO_2, 1150 °C	586	[54]
ABW_800	469.6	Corn stover	50% CO_2, 1150 °C	333	[54]
ABW_900	891.5	Walnut shells	99.9% CO_2, 900 °C	765	[55]
ABW_1000	623.5	Pelletized pine sawdust	O_2/steam, 800 °C	235–268	[56]
ABH_800	256.0	Pinewood	Steam, 800, 850 and 900 °C	364–889	[57]
ABH_900	419.1	Olive stone	99.9% CO_2, 800 °C	1355	[58]
ABH_1000	269.2				
WBP_800	520.9	Activated carbon			
WBP_900	748.9	Activated carbon		984	[23]
WBP_1000	764.8	Activated carbon		1002	[23]

3.2.2. Morphology of Raw Biomass and Chars

The surface morphology and structure of the studied samples is presented in Figure 5. In this analysis, the raw samples were chosen as a reference and the chars obtained at a temperature of 1000 °C were selected, due to the fact that the chars obtained at this temperature represent various surface areas according to the BET analysis. In the case of raw agricultural biomasses, the sample structure is more homogenous and fibrous, closed without noticeable pores. After physical activation by CO_2-gasification, the surface revealed an expanded and heterogeneous structure reached with a combination of micropores and mesopores. The ABW_1000 sample consists of sponge construction with irregular shapes and sizes, the surface area for these samples was 623 m^2/g, which indicates that it is still a high value. In case of ABH_1000, S_{BET} obtained the lowest value (269 m^2/g), its morphology is characterized by small holes as well as irregular shapes. Sample WBP_1000 enriched its structure in ordered and regular pores shape and sizes. The surface area of this sample obtained the highest value under 1000 °C. All char samples indicated similarities with the shapes to the parent materials. The release of volatile matter during gasification did not involve damage to the structure of the char particles due to the natural porosity of the biomass [59]. On the other hand, rapid release of volatile compounds at high temperature leads to the softening of the solid matrix or a coverage of the pores by fractional melt formation [60], which then causes clogging of the pores. High-temperature releases additional volatiles, which cannot be exhausted because of

closed pores. Overpressure is generated in the samples, resulting in the formation of bubbles, cracks and finally fragmentation [61]. Kamble et al. reported similar behavior of biomass char structure in [62].

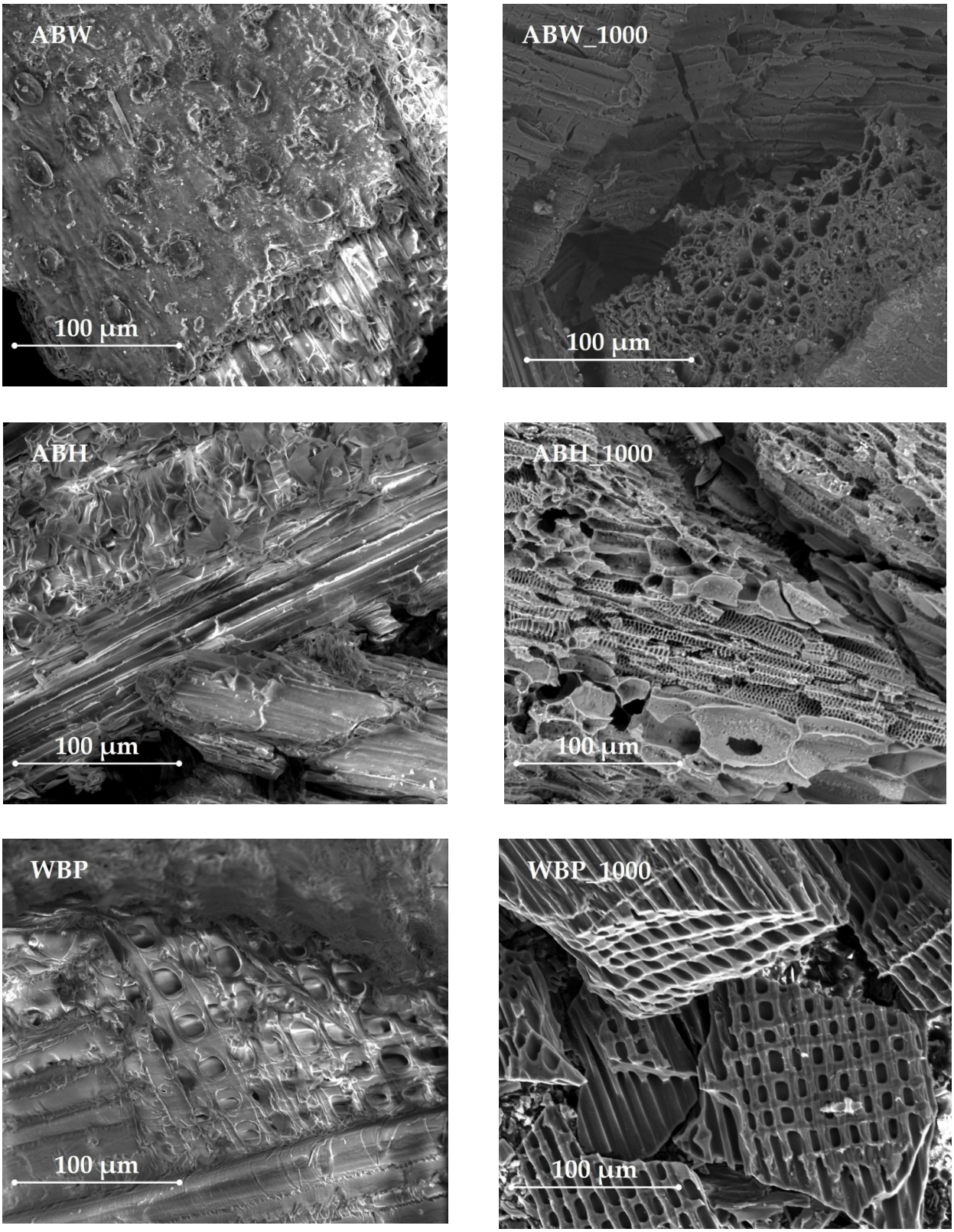

Figure 5. SEM images of the raw biomasses (ABW, ABH, and WBP) and their chars (ABW_1000, ABH_1000, and WBP_1000).

3.2.3. Surface Functional Groups

The FTIR spectra for raw biomass and chars obtained at 900 °C are presented in Figure 6. The results indicate a difference in the FTIR spectrum, where the main peaks appearing in the raw sample after the gasification process did not occur in the char analysis. This phenomenon is related to the decomposition of chemical compounds caused by gasification, and it can be seen by flattening out in the transmittance bands. The first main peak in raw material occurred between 3200 and 3600 cm^{-1}, which corresponded to the hydrogen-bonded O-H stretch, where spectra from approximately 2920 and 2850 cm^{-1} indicated the symmetric/asymmetric stretch of methylene CH. The alkenyl stretch C=C was recognized with a wavenumber of approximately 1640 cm^{-1} [24]. Cellulose bonds C=O appeared at 1030 cm^{-1}; in the case of char ABH_900, we can see that this bond was not completely decomposed. According to the study by Sun et al. [63], samples with functional groups counting oxygen indicated high reactivity for graphene oxide adsorption. The thermal degradation of the chars and the reduction of the peaks compared to the raw materials indicate that an aromatic structure was formed during gasification [64,65].

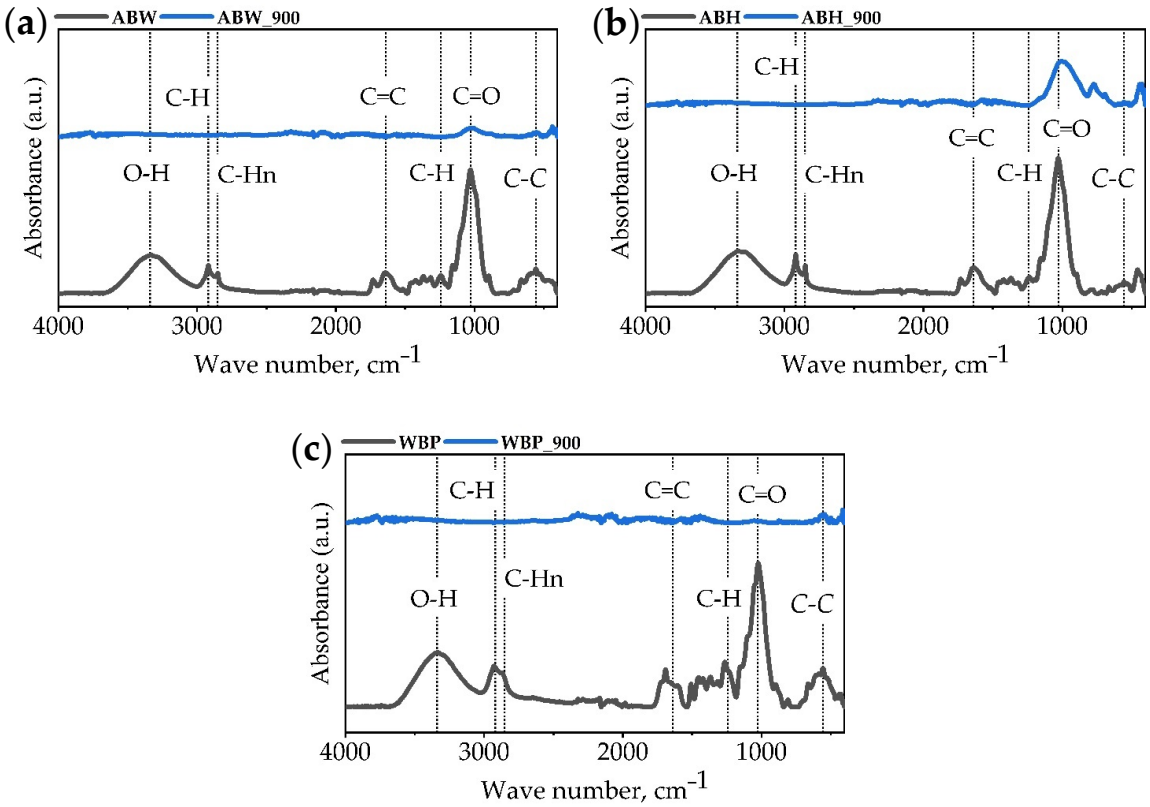

Figure 6. FTIR spectrum of (**a**) ABW, (**b**) ABH and (**c**) WBP.

3.2.4. Dynamic Methanol Vapor Sorption Tests

Methanol adsorption was analyzed to define potential utilization of produced solid residue as VOCs adsorbent or adsorbent in working pair in methanol in sorption cooling devices. The methanol intake was tested in an adsorption temperature 30 °C, and desorption temperature 60 °C, and the sorption isotherms are visualized in Figures 7–9.

The solid residues of ABW_900 in Figure 7 and WBP_900 in Figure 9 were characterized by an adsorption isotherm of type II, and a very small hysteresis of adsorption was observed, which confirms the microporous structure of the analyzed materials. However, a slight H4 type hysteresis might suggest the presence of split pores in the samples. Non-uniform tendency and weakest sorption capacity were observed for sample ABH_900 in Figure 8, which was also characterized by the lowest specific surface area equal to 419.1 m^2/g. However, most probably the results for this sample were not associated with the biomass type, but they

were disturbed by high soil contamination of the sample, as its ash content is 21.83%. Whereas, the ash content in hay reported in the literature is in the range of 6–8% [66,67].

Chars produced from wheat straw and wood (ABW and WBP) have exhibited a moderate methanol adsorption capacity, which was similar in both analyzed temperatures. Despite of the quite noticeable BET specific surface area of samples after gasification at 900 °C, the produced chars have shown average sorption properties. The highest weight gain was observed for the process temperature of 60 °C for the WBP_900 sample. For the value of P/P_0 of 90% the mass change was equal to 24.15%. Similar methanol uptakes were noted for commercial activated carbons (e.g., Norit GL 50) of BET not higher than 600 m^2/g. Other commercial, wood- and coal-based activated carbons of specific surface area equal to 1200 m^2/g present the maximal methanol sorption at the level not higher than 40% [68,69]. Unfortunately, the presented sorption properties do not present produced solid residue derived from biomass waste as most suitable candidates for a sorption chiller adsorbent. However, due to noticeable methanol sorption capacity and the origin of the studied material, produced solid residue might be a proper material for VOCs sorption [27] and subscribe in a circular economy concept.

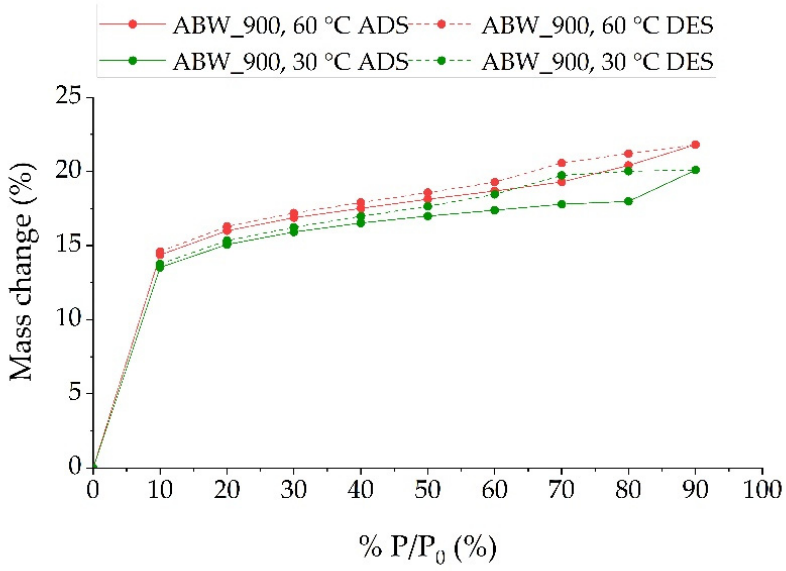

Figure 7. Adsorption and desorption isotherms for the samples ABW_900 at 30 and 60 °C.

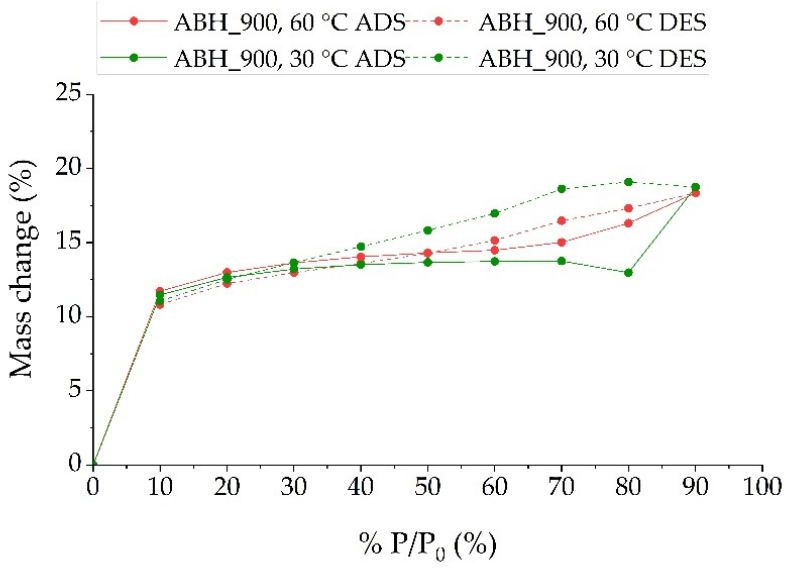

Figure 8. Adsorption and desorption isotherms for the sample ABH_900 at 30 and 60 °C.

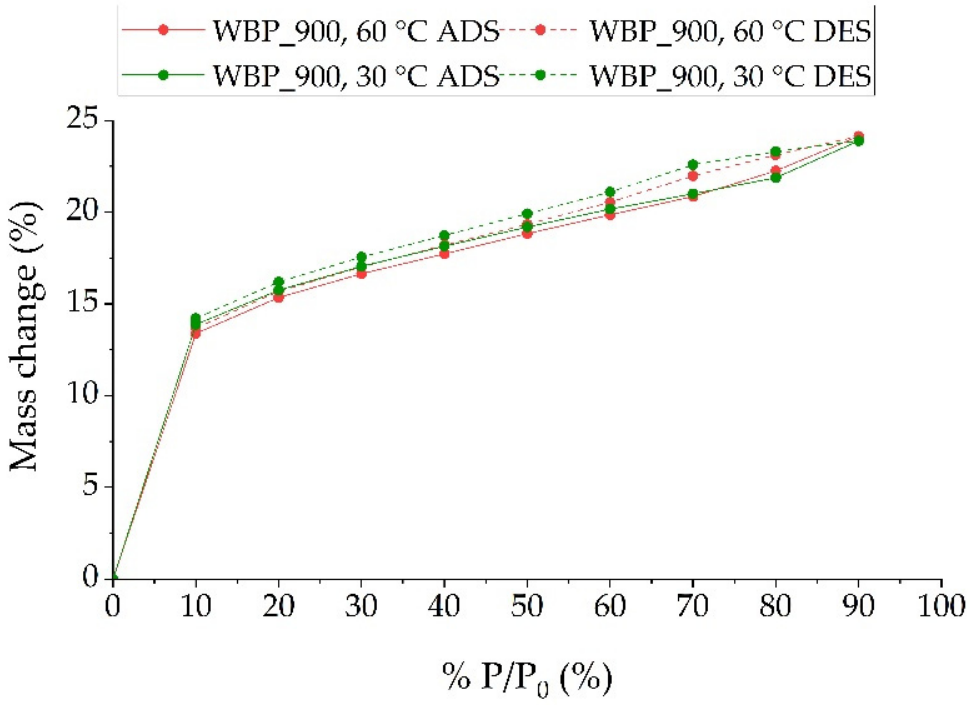

Figure 9. Adsorption and desorption isotherms for the sample WBP_900 at 30 and 60 °C.

4. Conclusions

The main conclusions of this study in agreement with the literature are as follows:

- The gasification process leads to an increase in the content of C in the char, with a parallel decrease in the concentration of H and O. This change affected the hydrogen (H/C ratio) and oxygen (O/C ratio) indexes, which both decreased significantly for the char samples. The above shift indicates that chars become more alike to coal. A similar trend was observed by analyzing the HHV value of the chars compared to the raw biomass;
- The TGA results for the combustion process of raw biomass and chars showed that the char samples lack peaks related to the burning of volatile matter. Additionally, key combustion parameters indicated that the chars have properties comparable to those of coal;
- The provided analysis of the chars obtained from waste biomass has proved similarities of these materials with coals, which confirms the possibility of using them energetically;
- The conducted gasification process leads to the formation of pores and cracks in the morphological structure of the chars, which results in the formation of the heterogeneous structure. Organic compounds were decomposed during the process, which is reflected by flattening out of the FTIR spectra;
- Chars significantly increased their specific surface area in comparison to raw materials. The highest increase is observed for the WBP sample, where the surface area of the raw sample is equal to 0.42 m^2/g, while a value of 764.8 m^2/g for WBP_1000 is determined, indicating that these materials are potential candidates for AC production; and
- Unfortunately, the studied samples are not the most applicable materials for the production of activated carbon (AC) used in working pairs with methanol in sorption chillers. On the other hand, the results indicated that the produced chars can be good candidates for VOCs sorption.

Author Contributions: Conceptualization, M.S., A.M. and A.M.-M.; data curation, M.S.; formal analysis, M.S., A.M., A.M.-M., I.K.-R., W.K. and F.K.; funding acquisition, M.S. and A.M.; investigation, M.S. and A.M.-M.; methodology, M.S., A.M., I.K.-R., W.K. and F.K.; project administration M.S. and A.M.; resources, M.S., A.M.-M., I.K.-R., A.M., F.K., M.R. and W.K.; supervision, A.M. and M.R.; validation, M.S., A.M. and A.M.-M.; writing—original draft, M.S. and A.M.-M.; writing—review & editing, A.M., F.K. and M.R. All authors have read and agreed to the published version of the manuscript.

Funding: Part of this work was supported by the Ministry of Science and Higher Education, Poland (grant AGH UST no 16.16.110.663) and co-financed by the European Union from the European Social Fund under the project: POWR.03.05.00-00-Z307/17-00.

Institutional Review Board Statement: Not applicable.

Informed Consent Statement: Not applicable.

Data Availability Statement: Not applicable.

Conflicts of Interest: The authors declare no conflict of interest.

References

1. Greiner, P.T.; York, R.; McGee, J.A. When are fossil fuels displaced? An exploratory inquiry into the role of nuclear electricity production in the displacement of fossil fuels. *Heliyon* **2022**, *8*, e08795. [CrossRef]
2. Syberg, K.; Nielsen, M.B.; Oturai, N.B.; Clausen, L.P.W.; Ramos, T.M.; Hansen, S.F. Circular economy and reduction of micro(nano)plastics contamination. *J. Hazard. Mater. Adv.* **2022**, *5*, 100044. [CrossRef]
3. Ansari, K.B.; Kamal, B.; Beg, S.; Wakeel Khan, M.A.; Khan, M.S.; Al Mesfer, M.K.; Danish, M. Recent developments in investigating reaction chemistry and transport effects in biomass fast pyrolysis: A review. *Renew. Sustain. Energy Rev.* **2021**, *150*, 111454. [CrossRef]
4. Maniscalco, M.; Infurna, G.; Caputo, G.; Botta, L.; Dintcheva, N.T. Slow pyrolysis as a method for biochar production from carob waste: Process investigation and products' characterization. *Energies* **2021**, *14*, 8457. [CrossRef]
5. Czerwińska, K.; Śliz, M.; Wilk, M. Hydrothermal carbonization process: Fundamentals, main parameter characteristics and possible applications including an effective method of SARS-CoV-2 mitigation in sewage sludge. A review. *Renew. Sustain. Energy Rev.* **2022**, *154*, 111873. [CrossRef]
6. Han, S.; Bai, L.; Chi, M.; Xu, X.; Chen, Z.; Yu, K. Conversion of Waste Corn Straw to Value-Added Fuel via Hydrothermal Carbonization after Acid Washing. *Energies* **2022**, *15*, 1828. [CrossRef]
7. Yu, J.; Guo, Q.; Gong, Y.; Ding, L.; Wang, J.; Yu, G. A review of the effects of alkali and alkaline earth metal species on biomass gasification. *Fuel Process. Technol.* **2021**, *214*, 106723. [CrossRef]
8. Vishwajeet, V.; Pawlak-Kruczek, H.; Baranowski, M.; Czerep, M.; Chorążyczewski, A.; Krochmalny, K.; Ostrycharczyk, M.; Ziółkowski, P.; Madejski, P.; Mączka, T.; et al. Entrained Flow Plasma Gasification of Sewage Sludge–Proof-of-Concept and Fate of Inorganics. *Energies* **2022**, *15*, 1948. [CrossRef]
9. Zhang, W.; Wu, Y.; Huang, S.; Wu, S.; Gao, J. Study on physicochemical characteristics, solidification and utilisation of tannery sludge gasification ash. *J. Environ. Manag.* **2022**, *310*, 114584. [CrossRef]
10. Yayalık, İ.; Koyun, A.; Akgün, M. Gasification of Municipal Solid Wastes in Plasma Arc Medium. *Plasma Chem. Plasma Process.* **2020**, *40*, 1401–1416. [CrossRef]
11. Lv, L.; Zhang, Z.; Li, H. SNG-electricity cogeneration through MSW gasification integrated with a dual chemical looping process. *Chem. Eng. Process.—Process Intensif.* **2019**, *145*, 107665. [CrossRef]
12. Razmi, A.R.; Heydari Afshar, H.; Pourahmadiyan, A.; Torabi, M. Investigation of a combined heat and power (CHP) system based on biomass and compressed air energy storage (CAES). *Sustain. Energy Technol. Assess.* **2021**, *46*, 101253. [CrossRef]
13. Ahmad, A.A.; Zawawi, N.A.; Kasim, F.H.; Inayat, A.; Khasri, A. Assessing the gasification performance of biomass: A review on biomass gasification process conditions, optimization and economic evaluation. *Renew. Sustain. Energy Rev.* **2016**, *53*, 1333–1347. [CrossRef]
14. Hasanzadeh, R.; Azdast, T.; Mojaver, M.; Park, C.B. High-efficiency and low-pollutant waste polystyrene and waste polystyrene foam gasification: Comprehensive comparison analysis, multi-objective optimization and multi-criteria decision analysis. *Fuel* **2022**, *316*, 123362. [CrossRef]
15. Benedetti, V.; Patuzzi, F.; Baratieri, M. Characterization of char from biomass gasification and its similarities with activated carbon in adsorption applications. *Appl. Energy* **2018**, *227*, 92–99. [CrossRef]
16. Nguyen, H.N.; Khuong, D.A.; Tran-Nguyen, P.L.; Tsubota, T. Towards sustainable biomass gasification: Evolution of bagasse char characteristics throughout gasification. *Biomass Bioenergy* **2022**, *158*, 106384. [CrossRef]

17. Naji, S.Z.; Tye, C.T. A review of the synthesis of activated carbon for biodiesel production: Precursor, preparation, and modification. *Energy Convers. Manag. X* **2022**, *13*, 100152. [CrossRef]
18. Narowska, B.E.; Kułażyński, M.; Łukaszewicz, M. Application of activated carbon to obtain biodiesel from vegetable oils. *Catalysts* **2020**, *10*, 1049. [CrossRef]
19. Sadeek, S.A.; Mohammed, E.A.; Shaban, M.; Abou Kana, M.T.H.; Negm, N.A. Synthesis, characterization and catalytic performances of activated carbon-doped transition metals during biofuel production from waste cooking oils. *J. Mol. Liq.* **2020**, *306*, 112749. [CrossRef]
20. Mazlan, M.A.F.; Uemura, Y.; Yusup, S.; Elhassan, F.; Uddin, A.; Hiwada, A.; Demiya, M. Activated Carbon from Rubber Wood Sawdust by Carbon Dioxide Activation. *Procedia Eng.* **2016**, *148*, 530–537. [CrossRef]
21. Phiri, Z.; Everson, R.C.; Neomagus, H.W.J.P.; Wood, B.J. The effect of acid demineralising bituminous coals and de-ashing the respective chars on nitrogen functional forms. *J. Anal. Appl. Pyrolysis* **2017**, *125*, 127–135. [CrossRef]
22. Subramani, T.; Revathi, P.K. Production of Activated Carbon from Agricultural Raw Waste. *IOSR J. Eng.* **2015**, *5*, 54–63.
23. Benedetti, V.; Cordioli, E.; Patuzzi, F.; Baratieri, M. CO_2 Adsorption study on pure and chemically activated chars derived from commercial biomass gasifiers. *J. CO_2 Util.* **2019**, *33*, 46–54. [CrossRef]
24. Jung, H.; Sewu, D.D.; Ohemeng-Boahen, G.; Lee, D.S.; Woo, S.H. Characterization and adsorption performance evaluation of waste char by-product from industrial gasification of solid refuse fuel from municipal solid waste. *Waste Manag.* **2019**, *91*, 33–41. [CrossRef]
25. Marchelli, F.; Cordioli, E.; Patuzzi, F.; Sisani, E.; Barelli, L.; Baratieri, M.; Arato, E.; Bosio, B. Experimental study on H_2S adsorption on gasification char under different operative conditions. *Biomass Bioenergy* **2019**, *126*, 106–116. [CrossRef]
26. Barontini, F.; Frigo, S.; Gabbrielli, R.; Sica, P. Co-gasification of woody biomass with organic and waste matrices in a down-draft gasifier: An experimental and modeling approach. *Energy Convers. Manag.* **2021**, *245*, 114566. [CrossRef]
27. Zhou, C.; Zhou, K.; Li, H.; Xu, X.; Liu, B.; Li, H.; Zeng, Z.; Ma, W.; Li, L. Pressure swing adsorption properties of activated carbon for methanol, acetone and toluene. *Chem. Eng. J.* **2021**, *413*, 127384. [CrossRef]
28. Friedl, A.; Padouvas, E.; Rotter, H.; Varmuza, K. Prediction of heating values of biomass fuel from elemental composition. *Anal. Chim. Acta* **2005**, *544*, 191–198. [CrossRef]
29. Shmroukh, A.N.; Ali, A.H.H.; Ookawara, S. Adsorption working pairs for adsorption cooling chillers: A review based on adsorption capacity and environmental impact. *Renew. Sustain. Energy Rev.* **2015**, *50*, 445–456. [CrossRef]
30. Jerai, F.; Miyazaki, T.; Saha, B.B.; Koyama, S. Overview of adsorption cooling system based on activated carbon—Alcohol pair. *Evergreen* **2015**, *2*, 30–40. [CrossRef]
31. Sur, A.; Das, R.K. Experimental investigation on waste heat driven activated carbon-methanol adsorption cooling system. *J. Braz. Soc. Mech. Sci. Eng.* **2017**, *39*, 2735–2746. [CrossRef]
32. Sztekler, K.; Kalawa, W.; Mika, Ł.; Mlonka-Medrala, A.; Sowa, M.; Nowak, W. Effect of additives on the sorption kinetics of a silica gel bed in adsorption chiller. *Energies* **2021**, *14*, 1083. [CrossRef]
33. Sztekler, K.; Mlonka-Mędrala, A.; Khdary, N.H.; Kalawa, W.; Nowak, W.; Mika, Ł. Possibility of Advanced Modified-Silica-Based Porous Materials Utilisation in Water Adsorption Processes—A Comparative Study. *Energies* **2022**, *15*, 368. [CrossRef]
34. Munir, S.; Daood, S.S.; Nimmo, W.; Cunliffe, A.M.; Gibbs, B.M. Thermal analysis and devolatilization kinetics of cotton stalk, sugar cane bagasse and shea meal under nitrogen and air atmospheres. *Bioresour. Technol.* **2009**, *100*, 1413–1418. [CrossRef] [PubMed]
35. Ren, J.; Cao, J.P.; Zhao, X.Y.; Liu, Y.L. Fundamentals and applications of char in biomass tar reforming. *Fuel Process. Technol.* **2021**, *216*, 106782. [CrossRef]
36. Singh, M.; Salaudeen, S.A.; Gilroyed, B.H.; Dutta, A. Simulation of biomass-plastic co-gasification in a fluidized bed reactor using Aspen plus. *Fuel* **2022**, *319*, 123708. [CrossRef]
37. González-Vázquez, M.P.; García, R.; Gil, M.V.; Pevida, C.; Rubiera, F. Comparison of the gasification performance of multiple biomass types in a bubbling fluidized bed. *Energy Convers. Manag.* **2018**, *176*, 309–323. [CrossRef]
38. Wang, G.; Zhang, J.; Huang, X.; Liang, X.; Ning, X.; Li, R. Co-gasification of petroleum coke-biomass blended char with steam at temperatures of 1173–1373 K. *Appl. Therm. Eng.* **2018**, *137*, 678–688. [CrossRef]
39. Noushabadi, A.S.; Dashti, A.; Ahmadijokani, F.; Hu, J.; Mohammadi, A.H. Estimation of higher heating values (HHVs) of biomass fuels based on ultimate analysis using machine learning techniques and improved equation. *Renew. Energy* **2021**, *179*, 550–562. [CrossRef]
40. Wang, Z.; Burra, K.G.; Li, X.; Zhang, M.; He, X.; Lei, T.; Gupta, A.K. CO_2-assisted gasification of polyethylene terephthalate with focus on syngas evolution and solid yield. *Appl. Energy* **2020**, *276*, 115508. [CrossRef]
41. Zhang, X.; Zhu, S.; Zhu, J.; Lyu, Q.; Wei, K.; Huang, Q.; Li, G.; Xia, H. TG-MS study on co-combustion characteristics and coupling mechanism of coal gasification fly ash and coal gangue by ECSA®. *Fuel* **2022**, *314*, 123086. [CrossRef]
42. Ding, H.; Ouyang, Z.; Wang, W.; Zhang, X.; Zhu, S. Experimental study on the influence of O_2/CO_2 ratios on NO conversion and emission during combustion and gasification of high-temperature coal char. *Fuel* **2022**, *310*, 122311. [CrossRef]

43. Guo, Y.; Guo, F.; Zhou, L.; Guo, Z.; Miao, Z.; Liu, H.; Zhang, X.; Wu, J.; Zhang, Y. Investigation on co-combustion of coal gasification fine slag residual carbon and sawdust char blends: Physiochemical properties, combustion characteristic and kinetic behavior. *Fuel* **2021**, *292*, 120387. [CrossRef]
44. Sieradzka, M.; Gao, N.; Quan, C.; Mlonka-Mędrala, A.; Magdziarz, A. Biomass thermochemical conversion via pyrolysis with integrated CO_2 capture. *Energies* **2020**, *13*, 1050. [CrossRef]
45. Sieradzka, M.; Kirczuk, C.; Kalemba-Rec, I.; Mlonka-Mędrala, A.; Magdziarz, A. Pyrolysis of Biomass Wastes into Carbon Materials. *Energies* **2022**, *15*, 1941. [CrossRef]
46. Ma, B.G.; Li, X.G.; Xu, L.; Wang, K.; Wang, X.G. Investigation on catalyzed combustion of high ash coal by thermogravimetric analysis. *Thermochim. Acta* **2006**, *445*, 19–22. [CrossRef]
47. Lu, J.J.; Chen, W.H. Investigation on the ignition and burnout temperatures of bamboo and sugarcane bagasse by thermogravimetric analysis. *Appl. Energy* **2015**, *160*, 49–57. [CrossRef]
48. Liu, Y.; Cao, X.; Duan, X.; Wang, Y.; Che, D. Thermal analysis on combustion characteristics of predried dyeing sludge. *Appl. Therm. Eng.* **2018**, *140*, 158–165. [CrossRef]
49. Niu, S.L.; Lu, C.M.; Han, K.H.; Zhao, J.L. Thermogravimetric analysis of combustion characteristics and kinetic parameters of pulverized coals in oxy-fuel atmosphere. *J. Therm. Anal. Calorim.* **2009**, *98*, 267–274. [CrossRef]
50. Li, X.G.; Lv, Y.; Ma, B.G.; Jian, S.W.; Tan, H.B. Thermogravimetric investigation on co-combustion characteristics of tobacco residue and high-ash anthracite coal. *Bioresour. Technol.* **2011**, *102*, 9783–9787. [CrossRef]
51. Reinmöller, M.; Sieradzka, M.; Laabs, M.; Schreiner, M.; Mlonka-Mędrala, A.; Kopia, A.; Meyer, B.; Magdziarz, A. Investigation of the thermal behaviour of different biomasses and properties of their low- and high-temperature ashes. *Fuel* **2021**, *301*, 121026. [CrossRef]
52. Mureddu, M.; Dessì, F.; Orsini, A.; Ferrara, F.; Pettinau, A. Air- and oxygen-blown characterization of coal and biomass by thermogravimetric analysis. *Fuel* **2018**, *212*, 626–637. [CrossRef]
53. Xu, M.X.; Wu, Y.C.; Nan, D.H.; Lu, Q.; Yang, Y.P. Effects of gaseous agents on the evolution of char physical and chemical structures during biomass gasification. *Bioresour. Technol.* **2019**, *292*, 121994. [CrossRef] [PubMed]
54. Wu, R.; Beutler, J.; Price, C.; Baxter, L.L. Biomass char particle surface area and porosity dynamics during gasification. *Fuel* **2020**, *264*, 116833. [CrossRef]
55. Jung, S.H.; Oh, S.J.; Choi, G.G.; Kim, J.S. Production and characterization of microporous activated carbons and metallurgical bio-coke from waste shell biomass. *J. Anal. Appl. Pyrolysis* **2014**, *109*, 123–131. [CrossRef]
56. Chen, T.; Zhang, J.; Wang, Z.; Zhao, R.; He, J.; Wu, J.; Qin, J. Oxygen-enriched gasification of lignocellulosic biomass: Syngas analysis, physicochemical characteristics of the carbon-rich material and its utilization as an anode in lithium ion battery. *Energy* **2020**, *212*, 118771. [CrossRef]
57. Alvarez, J.; Lopez, G.; Amutio, M.; Bilbao, J.; Olazar, M. Evolution of biomass char features and their role in the reactivity during steam gasification in a conical spouted bed reactor. *Energy Convers. Manag.* **2019**, *181*, 214–222. [CrossRef]
58. Guerrero-Pérez, M.O.; Valero-Romero, M.J.; Hernández, S.; Nieto, J.M.L.; Rodríguez-Mirasol, J.; Cordero, T. Lignocellulosic-derived mesoporous materials: An answer to manufacturing non-expensive catalysts useful for the biorefinery processes. *Catal. Today* **2012**, *195*, 155–161. [CrossRef]
59. Khasraw, D.; Theint Htet, T.; Yang, X.; Degirmenci, V.; Hage, H.; Meijer, K.; Li, Z. Gasification and structural behaviour of different carbon sources and resultant chars from rapid devolatilization for HIsarna alternative ironmaking process. *Fuel* **2022**, *309*, 122210. [CrossRef]
60. Reinmöller, M.; Schreiner, M.; Guhl, S.; Neuroth, M.; Meyer, B. Formation and transformation of mineral phases in various fuels studied by different ashing methods. *Fuel* **2017**, *202*, 641–649. [CrossRef]
61. Biagini, E.; Simone, M.; Tognotti, L. Characterization of high heating rate chars of biomass fuels. *Proc. Combust. Inst.* **2009**, *32*, 2043–2050. [CrossRef]
62. Kamble, A.D.; Mendhe, V.A.; Chavan, P.D.; Saxena, V.K. Insights of mineral catalytic effects of high ash coal on carbon conversion in fluidized bed Co-gasification through FTIR, XRD, XRF and FE-SEM. *Renew. Energy* **2022**, *183*, 729–751. [CrossRef]
63. Sun, J.; Liu, X.; Duan, S.; Alsaedi, A.; Zhang, F.; Hayat, T.; Li, J. The influential factors towards graphene oxides removal by activated carbons: Activated functional groups vs. BET surface area. *J. Mol. Liq.* **2018**, *271*, 142–150. [CrossRef]
64. Pelaez-Samaniego, M.R.; Perez, J.F.; Ayiania, M.; Garcia-Perez, T. Chars from wood gasification for removing H_2S from biogas. *Biomass Bioenergy* **2020**, *142*, 105754. [CrossRef]
65. Rubio-Clemente, A.; Gutiérrez, J.; Henao, H.; Melo, A.M.; Pérez, J.F.; Chica, E. Adsorption capacity of the biochar obtained from Pinus patula wood micro-gasification for the treatment of polluted water containing malachite green dye. *J. King Saud Univ.—Eng. Sci.* 2021; *in press*. [CrossRef]
66. Zając, G.; Szyszlak-Bargłowicz, J.; Gołębiowski, W.; Szczepanik, M. Chemical characteristics of biomass ashes. *Energies* **2018**, *11*, 2885. [CrossRef]
67. Kraszkiewicz, A.; Kachel-Jakubowska, M.; Lorencowicz, E.; Przywara, A. Influence of Cellulose Content in Plant Biomass on Selected Qualitative Traits of Pellets. *Agric. Agric. Sci. Procedia* **2015**, *7*, 125–130. [CrossRef]

68. Gordeeva, L.; Aristov, Y. Dynamic study of methanol adsorption on activated carbon ACM-35.4 for enhancing the specific cooling power of adsorptive chillers. *Appl. Energy* **2014**, *117*, 127–133. [CrossRef]
69. Wu, J.W.; Madani, S.H.; Biggs, M.J.; Phillip, P.; Lei, C.; Hu, E.J. Characterizations of Activated Carbon-Methanol Adsorption Pair Including the Heat of Adsorptions. *J. Chem. Eng. Data* **2015**, *60*, 1727–1731. [CrossRef]